

On the Acid–Base Chemistry of Permanently Charged Minerals

ANNE M. L. KRAEPIEL*

Department of Chemistry, Frick Chemical Laboratory,
Princeton University, Princeton, New Jersey 08544

KLAUS KELLER

Department of Civil Engineering and Operations Research,
Princeton University, Princeton, New Jersey 08544

FRANÇOIS M. M. MOREL

Department of Geosciences, Guyot Hall, Princeton University,
Princeton, New Jersey 08544

The acid–base properties of oxides are well described by the surface complexation model, which superposes a thermodynamic description of acid–base reactions at the oxide surface with a double-layer model of the electrostatics at the solid–solution interface. So far, however, this model has not been extended to include the effects of permanent charges such as result, for example, from isomorphous substitution in clays. Contrary to oxides, solids with permanent charge often exhibit an increasing degree of protonation with decreasing ionic strength at low pH. They also show an increase in their zero proton condition (ZPC) with decreasing ionic strength. Here we examine the influence of the pH-independent charge of a solid on its acid–base properties. We consider two simple cases: model 1 in which all the acid–base groups and pH-independent charges are distributed at the surface of a nonpenetrable solid, at the interface with the solution; Model 2 in which the solid is porous (i.e., penetrable by water and electrolyte ions), and the pH-independent charges are distributed inside the bulk of the solid, while the acid–base groups are on the surface of the solid. For model 1, the Gouy–Chapman theory yields the surface potential as a function of surface charge and ionic strength; for model 2, the solution to the Poisson–Boltzmann equation applied both inside and outside the solid yields expressions for the internal and surface potentials as a function of internal charge, surface charge, and ionic strength. When these equations are used with reasonable physical and chemical parameters for models 1 and 2, the resulting acid–base calculations exhibit the same qualitative behavior as observed experimentally for clays. Models 1 and 2 are then shown to describe parsimoniously published acid–base titration data for kaolinite and montmorillonite, respectively.

Introduction

One of the important scientific contributions of Werner Stumm is his leadership in the conception, development, and promulgation of the *surface complexation model*. This

* Corresponding author telephone: (609)258-1052; fax: (609)258-5242; e-mail: kraepiel@geo.princeton.edu.

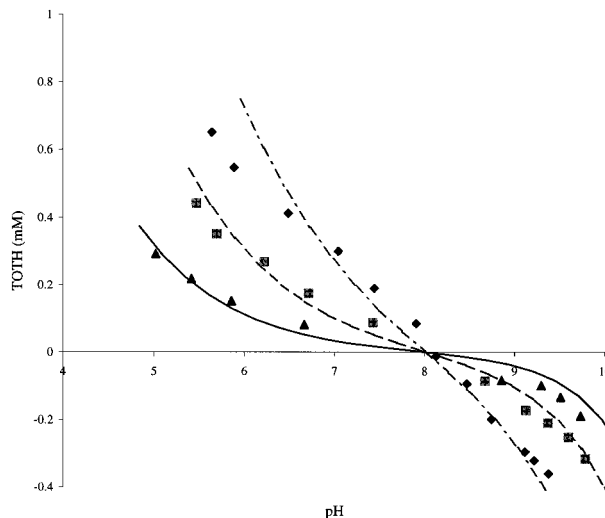


FIGURE 1. Acid–base titration curves for hydrous ferric oxide (HFO) at three different ionic strengths. Triangles and —: $I = 0.001$ M; squares and - - -: $I = 0.01$ M; diamonds and - · - ·: $I = 0.1$ M. The data points (symbols) are from Hsi and Langmuir (47). The model fits (lines) are obtained for the parameters described in Tables 1 and 2 using the surface complexation model [the generalized two-layer model, following Dzombak and Morel (4)]. TOH is defined as $\text{TOH} = [\text{H}^+] - [\text{OH}^-] + [\text{=SOH}_2^+] - [\text{=SO}^-]$ (see text for notation).

now well-accepted model superposes an essentially chemical view of the solid–water interface, described by reactive surface groups, with the physical description of the electrostatics of the interface provided by the classic theories of Gouy and Chapman (1, 2) and Stern (3). The senior author recalls that an early manifesto of the surface complexation revolution was a sketch on a napkin from Anthony Pier 4 in Boston, signed by Werner Stumm, Jim Morgan, Paul Schindler, and himself—in 1975—and retained by Stumm for use in future propaganda.

A central aspect of the surface complexation model is the recognition that the electrostatic charge developed on the surface of solids such as oxides results chiefly from acid–base reactions. The variations in the surface charge as a function of pH and ionic strength (see Figure 1) can then be explained quantitatively by describing the extent of acid–base reactions at the surface with simple mass law equations that include an explicit Coulombic term. This Coulombic term is effectively an activity coefficient for the surface species that takes into account the effect of the mean electrical potential at the surface on the energetics of the acid–base reactions (4).

As seen in Figure 1, a characteristic feature of acid–base titration data for oxides is that the titration curves at various ionic strengths all intersect at the same pH: the zero proton condition (ZPC), which in this case is also the point of zero charge (in the absence of other sorbing ions). This is an absolute necessity in the usual surface complexation model since all the effects of ionic strength on the acid–base properties of the surface are assumed to result from the variable shielding of Coulombic forces afforded by electrolyte ions. When there is no net charge, there is no Coulombic interaction, and there can be no effect of ionic strength.

The surface complexation model in various forms and extensions has now been applied successfully to describe reactions at the surface of many types of solids (5–7). There are important solids for which the application of the surface complexation model is, at best, uncomfortable however,

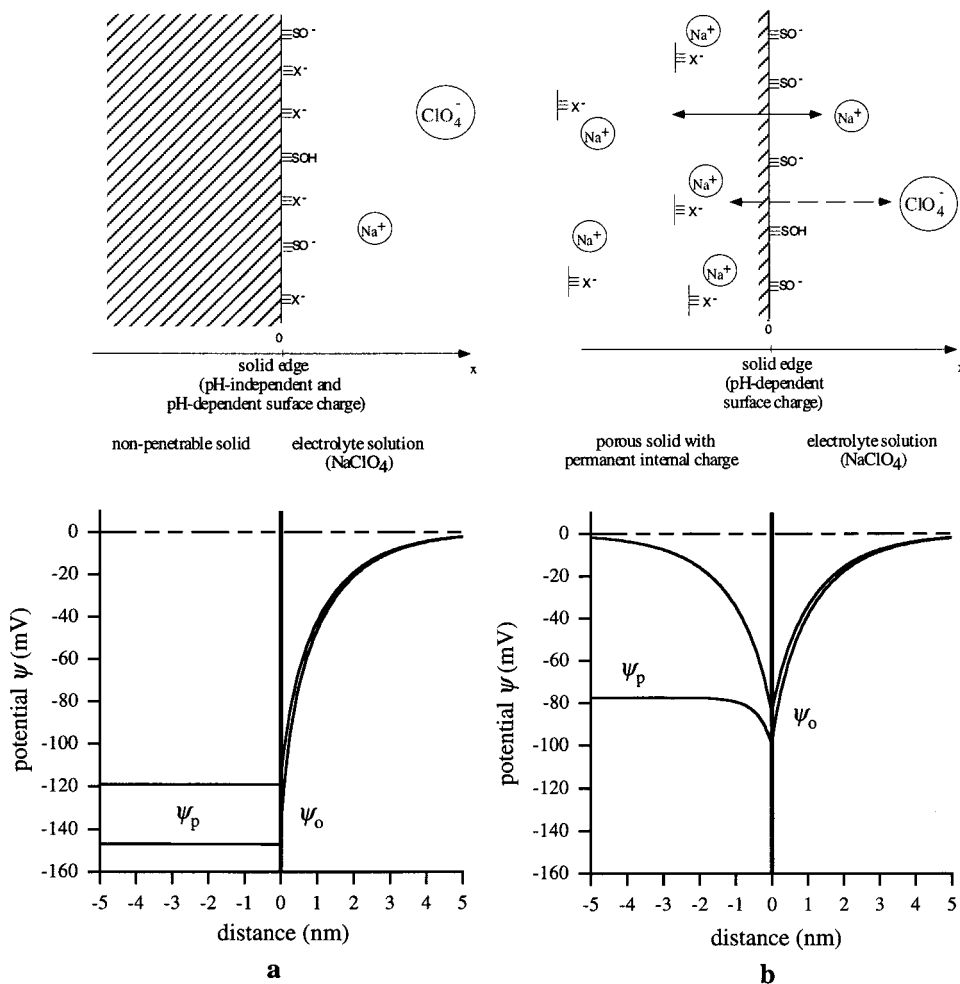


FIGURE 2. Two models of acid–base reactions on solids and of the variation of potential with distance from the solid–water interface; $I = 0.05 \text{ M}$. Panel a, Nonpenetrable solid with charged surface groups; permanent surface charge density = $-9.65 \times 10^{-2} \text{ C m}^{-2}$ (lower curve) and 0 (upper curve); surface charge density created by acid–base groups = -0.133 C m^{-2} . Panel b, Porous solid with permanent internal charge and amphoteric groups on the surface; permanent internal charge density = -1.02 equiv/L (lower curve) and 0 (upper curve), surface charge density = -0.133 C m^{-2} .

namely, those solids for which one observes variations of the ZPC with ionic strength. A prime example of such solids are clays—solids that usually possess permanent (i.e., pH-independent) charge because of isomorphous substitution of higher valence metal ions by lower valence ions (8, 9). Here, as an homage to Stumm and a testimony to the staying power of his ideas, we extend the surface complexation model to examine the acid–base chemistry of these solids.

Background

The relation between the electrical charge and potential at the surface of a nonpenetrable solid immersed in an electrolyte solution (Figure 2a) is given by the Gouy–Chapman—a k a double layer (DL)—theory (1, 2). (For simplicity, we consider only cases where the interface can be approximated by an infinite plane and the ionic strength of the solution is dominated by a 1:1 electrolyte.) The potential varies from the surface potential to its reference value in solution (= zero by convention) over distances of a few to a fraction of nanometers, depending on the ionic strength (I) of the solution. Because there is no electrical charge inside the solid, the electrical potential there is constant and fixed at the value of the surface potential (see Figure 2a).

If electrolyte ions can penetrate inside the solid, their distribution on both sides of the interface will be nonuniform, thus creating a double double-layer. The theory for the double double-layer (DDL) has been solved for a number of

different situations (10–16); we have previously treated the case of a porous solid with both a uniform bulk charge density (ρ_p) and a surface charge density, σ_o (17). In that case, the surface potential depends on ρ_p , σ_o , and I . At a great distance from the interface, it is zero in solution (reference value $\psi_{+\infty} = 0$) and in the solid ($\psi_{-\infty}$) it depends only on the internal charge density and the ionic strength of the solution. For high absolute values of ρ_p/I , it is given by the Donnan potential (18). On the solution side of the interface, the distribution of ions and the potential vary according to the Gouy–Chapman theory. As a result of the surface charge density, the surface potential may be lower or higher than the potential inside the bulk solid, and the variation in potential with distance is discontinuous at the interface as shown in Figure 2b.

Two models are developed to investigate the influence of a permanent negative charge, either on the surface of the solid or in the bulk, on the acid–base properties of solids:

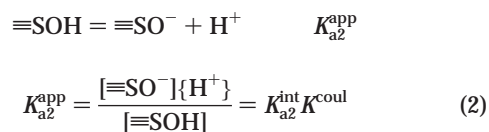
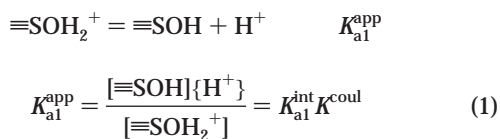
In model 1, corresponding to Figure 2a, the solid is nonpenetrable; its interface with the solution contains charged groups of two kinds: (i) X^- groups bearing a pH-independent charge, which provide the solid with a permanent (fixed) surface charge density (σ_{fix}); (ii) $\equiv\text{SOH}$ acid–base groups that can take or give protons and provide the solid with a variable surface charge density (σ_{var}). The surface charge density σ_o of the solid is the sum of the permanent and variable charge: $\sigma_o = \sigma_{\text{fix}} + \sigma_{\text{var}}$.

In model 2, corresponding to Figure 2b, the solid is porous, and the inside of the solid bears only pH-independent groups (X^-) distributed homogeneously inside the solid with a bulk charge density, ρ_p ; the internal electrolyte solution is represented as a homogeneous phase containing fixed point charges. Amphoteric acid–base groups ($\equiv\text{SOH}$) are located on the surface of the solid at the interface with the solution, resulting in a surface charge density σ_o .

Note: The units of ρ are in equivalent per liter of solution inside the solid, which we denote as equiv/L. Concentrations normalized to liters of external solution are written, for example, as mol/L.

Theory

Acid–Base Reactions at the Surface of the Solid. As in the usual surface complexation model, we describe the uptake or release of a proton as the reaction of an amphoteric acid–base group:



in which the brackets (e.g., $[\equiv\text{SOH}]$) denote the concentration of a given species in mol/L and $\{\text{H}^+\}$ is the activity of the hydrogen ion in solution. The Coulombic term in the equilibrium constant is calculated from the average surface potential ψ_o applicable to the reactive groups:

$$K^{\text{coul}} = e^{F\psi_o/RT} \quad (3)$$

where R is the gas constant ($8.314 \text{ J mol}^{-1} \text{ K}^{-1}$), T is the absolute temperature in Kelvin, and F is the Faraday constant in coulombs. The Coulombic term is pH-dependent and must be calculated explicitly in each equilibrium calculation on the basis of the double-layer theory or its extension as discussed below.

Cation Exchange in the Solid. In a porous solid bearing a negative internal charge, H^+ ions are sorbed by cation exchange. $[\text{H}^+]_p$, the number of moles of H^+ sorbed by cation exchange per volume of solution inside the solid (neglecting the activity coefficient), and $\{\text{H}^+\}$, the activity of H^+ in solution, are related by the following equation:

$$\frac{[\text{H}^+]_p}{\{\text{H}^+\}} = e^{-F\psi_p/RT} \quad (4)$$

where ψ_p is the potential inside the solid. Following Dzombak and Hudson (19), this relation may be represented as the mass law for the reaction of H^+ with a fictitious site whose activity is given by the right-hand side of eq 4. The potential ψ_p is calculated from the internal charge density (ρ_p) and the ionic strength (I) as described below.

Sorption in the Diffuse Layer(s). As can be seen in Figure 2, the variations in potential with distance inside the solid (obtained by numerical integration of the Poisson–Boltzmann equation) occur over distances that are similar or smaller than those in solution (obtained from the Gouy–Chapman theory). The effects of the variations in the distribution of ions near the interface (i.e., the two diffuse layers) on the net sorption of ions such as H^+ can thus be neglected in the case of the double double-layer as it can in

the case of the double-layer. For a porous sphere, it has been shown that the effects of the diffuse layers are only important if the diameter is less than 2 nm (16). We shall thus neglect adsorption in the double-layer(s).

Electrical Charge Density. The average potentials (ψ_o or ψ_p) result from a surface charge (σ_o) and/or an internal charge (ρ_p).

In model 1, for a nonpenetrable solid with $\equiv\text{SOH}$ and X^- groups on the surface of the solid, the surface charge density [σ_o (C m^{-2})] is calculated according to

$$\sigma_o = \frac{F([\equiv\text{SOH}_2^+] - [\equiv\text{SO}^-] - [X^-])}{\frac{m}{V_T}} \quad (5)$$

where m/V_T is the mass of dry solid per solution volume (kg/L) and s is the specific surface area of the solid (m^2/kg).

In model 2, for a porous solid with a pH-independent charge in the bulk and acid–base groups on the surface, the internal charge density [ρ_p (equiv/L)] is equal to

$$\rho_p = \frac{-[X^-]}{V_L/V_T} \quad (6)$$

in which V_L/V_T is the ratio of water volume inside the solid to the total solution volume. The surface charge density [σ_o (C m^{-2})] is calculated from

$$\sigma_o = \frac{F([\equiv\text{SOH}_2^+] - [\equiv\text{SO}^-])}{\frac{m}{V_T}} \quad (7)$$

Charge–Potential Relationship. Model 1: Nonpenetrable Solid with pH-Independent and pH-Dependent Surface Charge. In the case of a nonpenetrable solid with an infinite flat surface immersed in an electrolyte solution (double-layer theory, Figure 2a), the surface charge–surface potential relation has been derived by Gouy and Chapman (1, 2) as

$$\sigma_{oGC} = (8RT\epsilon_w\epsilon_o \times 1000)^{1/2} \times I^{1/2} \times \sin h(F\psi_o/2RT) \quad (8)$$

where σ_{oGC} (C m^{-2}) is the surface charge density and ψ_o (V) is the surface potential. ϵ_o is the vacuum permittivity ($8.854 \times 10^{-12} \text{ J}^{-1} \text{ C}^2 \text{ m}^{-1}$) and ϵ_w is the relative permittivity of the water.

Model 2: Porous Solid with both an Internal and a Surface Charge. As in the case of the Gouy–Chapman theory, we have assumed in this derivation (17) that the relation between charge and potential can be calculated from the Poisson–Boltzmann equation, which yields

in solution

$$\frac{d^2\psi}{dx^2} = -1000 \frac{FI(e^{-F\psi/RT} - e^{F\psi/RT})}{\epsilon_w\epsilon_o} \quad (9)$$

in the solid

$$\frac{d^2\psi}{dx^2} = -1000 \frac{F\rho_p + FI(e^{-F\psi/RT} - e^{F\psi/RT})}{\epsilon_s\epsilon_o \frac{V_p}{V_L}} \quad (10)$$

where ψ (V) is the potential, x (m) is the distance from the interface, and I (mol/L) is the electrolyte concentration. ϵ_s is the relative permittivity of the solid. V_p/V_L is the ratio of the total volume of solid to the solution volume inside the solid. The factor of 1000 is included to reconcile the units in meters and liters.

TABLE 1. Acid–Base Reactions of Amphoteric Species at the Interface Solid/Liquid

acid–base reactions	Figure 1 (HFO)	model 1	model 2
$\equiv\text{SOH}_2^+ = \equiv\text{SOH} + \text{H}^+$	$\log K_{a1}^{\text{int}} = -7.4$	$\log K_{a1}^{\text{int}} = -4.7$	$\log K_{a1}^{\text{int}} = -5.0$
$\equiv\text{SOH} = \equiv\text{SO}^- + \text{H}^+$	$\log K_{a2}^{\text{int}} = -8.6$	$\log K_{a2}^{\text{int}} = -8.6$	$\log K_{a2}^{\text{int}} = -8.5$

TABLE 2. Model Parameters

model parameters	Figure 1 (HFO)	model 1	model 2	source
surface area (edges) (m ² /kg)	6×10^5	2×10^5	3.15×10^4	HFO: ref 4 model 1: titration data model 2: BET (38)
$\epsilon_s(V_L/V_p)$	na ^a	na ^a	78.5	fixed equal to ϵ_w
concentration of acid–base groups (mol/kg)	2.25	1.75×10^{-2}	2.8×10^{-2}	HFO: ref 4 model 1 or 2: titration data
concentration of permanently charged surface groups (mol/kg)	na ^a	2.10^{-2}	na ^a	titration data
permanent internal charge density ρ_{fix} (equiv/L)	na ^a	na ^a	-1.02	fixed equal to $(m/V_L)\text{CEC}^b$
dry solid concentration, m/V_T (kg/L)	0.001	0.02	0.005	measured
ratio of dry solid mass to solution volume inside the solid, m/V_L (kg/L)	na ^a	na ^a	1	rounded off from ref 19

^a na, not applicable. ^b CEC, cation exchange capacity.

The internal potential in the solid is calculated from the internal charge density at infinite distance from the surface noting that

$$\left. \frac{d^2\psi}{dx^2} \right|_{-\infty} = \left. \frac{d\psi}{dx} \right|_{-\infty} = 0 \quad (11)$$

leading to

$$\psi_p = \frac{RT}{F} \arcsin h \left(\frac{\rho_p}{2I} \right) \quad (12)$$

which, for large potentials, reduces to the Donnan expression (18):

$$\psi_p = -\frac{RT}{F} \ln \left(\frac{-\rho_p}{I} \right) \quad (13)$$

The surface charge is given by the overall electroneutrality condition as

$$\sigma_{\text{ODDL}} = \epsilon_o \epsilon_s \left. \frac{d\psi}{dx} \right|_{x=0^-} - \epsilon_o \epsilon_w \left. \frac{d\psi}{dx} \right|_{x=0^+} = \sigma_{\text{op}} + \sigma_{\text{oGC}} \quad (14)$$

The surface charge–surface potential relationship is obtained by integrating eqs 9 and 10 for the same boundary condition $\psi = \psi_o$ at the surface. σ_{oGC} is given by eq 8 and σ_{op} is given by

$$\sigma_{\text{op}} = \text{sign} \left(\frac{8RT\epsilon_o}{2} \right)^{0.5} \left(\frac{\epsilon_s V_L}{V_p} \right)^{0.5} \left[1000I \left(\cosh \left(\frac{F\psi_o}{RT} \right) - \cosh \left(\frac{F\psi_p}{RT} \right) \right) + \frac{-1000\rho_p}{2} \frac{F}{RT} (\psi_o - \psi_p) \right]^{0.5} \quad (15)$$

where $\text{sign} = +1$ if $\psi_o > \psi_p$, and $\text{sign} = -1$ otherwise.

Methods

To calculate the effects of a pH-independent charge on the acid–base reactions of a solid according to the conditions described for models 1 and 2, it is necessary to solve simultaneously the mole balance equations for the acid–base species and the hydrogen ion, the mass laws equations, the equations for the surface and/or internal charge, and the

relevant potential–charge relation (either eqs 1, 2, 5, and 8 or eqs 1, 2, 4, 6, 7, 12 and 14). This is most easily achieved by using a computer program of the MINEQL family (20) in which the (exponential of the nondimensional) relevant potentials are included as dummy components following the method described by Westall (21). In the case of model 1, the equations are the same as the ones used in the usual surface complexation model, and the MINEQL⁺ 3.01a program distributed by W. D. Schecher (Environmental Research Software, 16 Middle St., Hallowell, ME 04347) can be used as such. In the case of model 2, however, both $X_p = e^{-F\psi_p/RT}$ and $X_o = e^{-F\psi_o/RT}$ are included as dummy components, and eqs 12 and 14 serve as the corresponding mole balance equivalents. Because the MINEQL programs use a Newton–Raphson iteration scheme, the differentials of all the mole balances with respect to all the components must be included in the program. This requires adding the differentials of eq 12 with respect to X_p and of eq 14 with respect to X_o to the relevant term in the Jacobian matrix. This was done by adding a subroutine, CLAYEQL (22), to the MINEQL⁺ 3.01a program. The parameters and the conditions used in the model calculations are given in Tables 1 and 2.

Results and Discussion

Model 1. We first examine the acid–base properties of a model solid containing both electrostatic permanent surface charges and acid–base groups at the interface with the solution according to the situation described in model 1. The only direct experimental information available on the acid–base chemistry of a solid is the variation in excess surface proton concentration as a function of solution parameters such as pH and ionic strength as shown in Figure 1. Such are the data that we wish ultimately to model and explain for clays. To gain insight into the processes that govern the acquisition or loss of protons by the solid, it is useful to first examine the distribution of acid–base species as a function of pH and ionic strength in the medium and the corresponding electrical potential that is calculated for the surface of the solid.

In the case where the permanent surface charge is zero or negligible, the log C–pH diagram of the surface acid–base species at high ionic strength resembles that of a normal diprotic acid (Figure 3b). As the ionic strength decreases

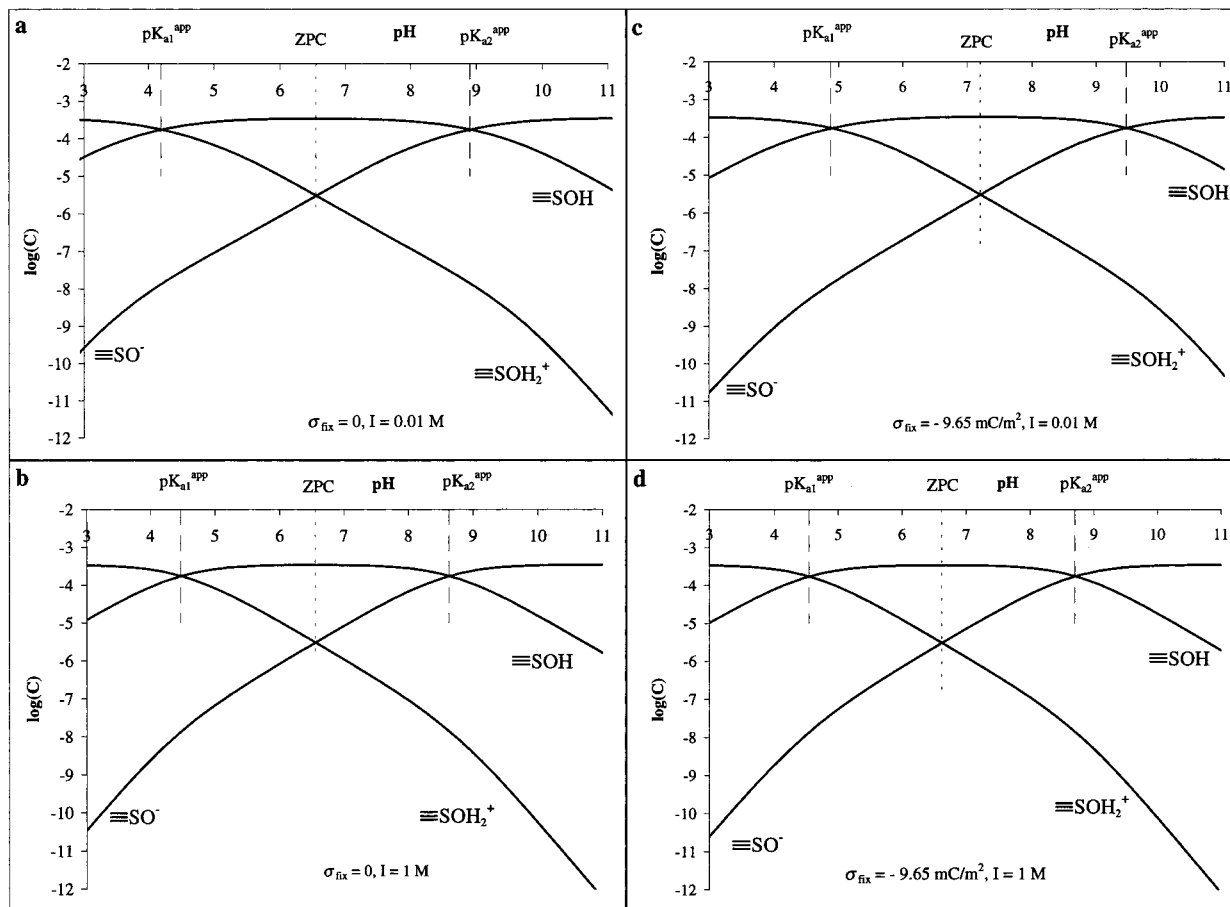


FIGURE 3. Log C –pH diagrams of acid–base species on the surface of a nonpenetrable solid with and without a permanent charge at the surface. Two different ionic strengths ($I = 0.01$ and 1 M) are represented. The model parameters are given in Tables 1 and 2. The scale, log C , is in moles per liter of solution (mol/L).

TABLE 3. Zero Proton Condition

	Figure 1 (HFO)	model 1	model 2
ZPC	$\frac{1}{2}(pK_{a1}^{int} + pK_{a2}^{int})$	$\frac{1}{2}(pK_{a1}^{int} + pK_{a2}^{int}) - \frac{1}{2.3} \frac{F\psi_{ZPC}}{RT}$	
$\frac{F\psi_{ZPC}}{RT}$	0	$2 \arcsin h\left(\frac{\sigma_{fix}}{0.1174I^{1/2}}\right)$	$\frac{2I}{\rho_p} \left(1 - \cosh\left(\frac{F\psi_p}{RT}\right)\right) + \frac{F\psi_p}{RT}$ ^a

^a Valid only if $\epsilon_S(V_L/V_P) = \epsilon_w$.

(Figure 3a), the ZPC remains constant (see Table 3), but the apparent pK_a values become increasingly separated. This is the well-known behavior for surface acid groups according to the surface complexation model (4, 23). The increasing separation of the apparent pK_a values results from the increasing repulsion (respectively attraction) of H^+ by the positive (respectively negative) charge when the concentration of shielding ions in the electrolyte solution becomes smaller.

The addition of a permanent negative charge density on the solid increases the ZPC as expected since, at any given pH, the Coulombic interactions increase the concentration of $\equiv SOH_2^+$ groups and decrease that of $\equiv SO^-$ groups as compared to the case with no permanent surface charge (Figure 3c). This effect is, of course, identical to that caused, for example, by the specific sorption of an anion on the surface of an oxide as discussed by Stumm and co-workers (23, 24). Because of the shielding of Coulombic forces by electrolyte ions, this effect is decreased at higher ionic strength (Figure

3d). Thus in the case of a solid bearing a permanent surface charge, unlike what is predicted by the usual surface complexation model, the ZPC depends on the ionic strength. Note that while the ZPC is dependent on the density of permanent surface charges (σ_{fix}), it is unaffected by the concentration of acid–base groups (see Table 3).

As seen in the mass law eqs 1 and 2, the variations in the log C –pH diagrams we just discussed are all caused by variations in the electrical potential. The variations of the surface potential with pH in turn depend on three parameters: (i) the surface charge density of pH-independent charges X^- (σ_{fix}), (ii) the concentration of acid–base groups $\equiv SOH$ (σ_{var}^{max}), and (iii) the ionic strength I (see Figure 4).

When there is no permanent surface charge, the surface potential varies with pH and ionic strength according to the well-known features described in detail by Dzombak and Morel (4): (i) at low ionic strength, the potential decreases from high to low values as pH increases; (ii) the amplitude of this variation is much decreased as I increases; and (iii)

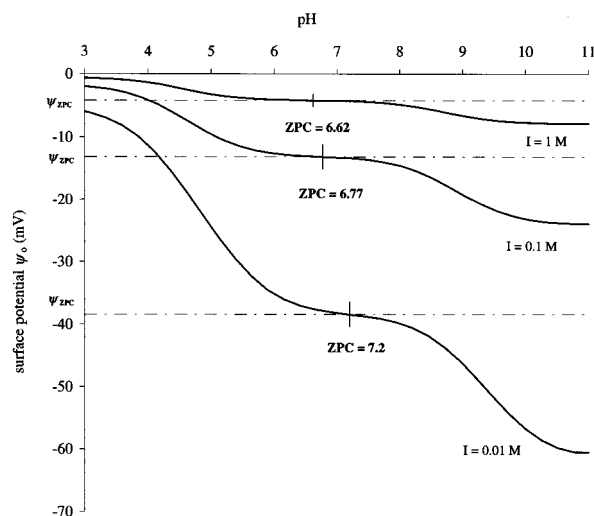


FIGURE 4. Surface potential versus pH at three ionic strengths ($I = 0.01, 0.1,$ and 1 M) for a nonpenetrable solid; the permanent surface charge density is $\sigma_{\text{fix}} = -9.65 \times 10^{-3}\text{ C m}^{-2}$. The model parameters are the same as for Figure 3. The dashed-dotted lines correspond to ψ_{ZPC} , the potential that would be created by the permanent charge alone.

the ψ vs pH curves at various I cross each other at the ZPC, where the surface potential (ψ_{ZPC}) is equal to zero.

When there is a permanent surface charge, ψ_{ZPC} is shifted to a negative value (see Table 3). This negative potential increases in magnitude at low ionic strengths. The potential at the ZPC is determined by the permanent charge density and the ionic strength, while the amplitude of the potential variation with pH is governed by the concentration of acid-base groups and the ionic strength. The ZPC depends only on the permanent charge density and is independent of the concentration in variable charge (but depends, of course, on the $\text{p}K_{\text{a}}$ values of the acid-base groups, see Table 3).

As a result, for a solid with both a permanent and variable surface charge, the potential vs pH curves at various I values do not cross each other at the ZPC (see Figure 4); in fact, they never intersect if, as is the case for Figure 4, σ_{fix} has a higher absolute value than $\sigma_{\text{var}}^{\text{max}}$. The potential vs pH curves are then dominated by the negative potential created by the permanent charge. Since this potential decreases rapidly (becomes more negative) with decreasing ionic strength, the potential vs pH curves for different ionic strengths become separated.

Application to Kaolinite. Kaolinite is a nonexpandable clay, made of a succession of gibbsite and siloxane sheets, and organized in 1:1 layers separated by interlayers; the layers are bound together by hydrogen bonding. It seems that water and electrolyte ions cannot penetrate in the interlayers (25, 26), although some authors have hypothesized that H^+ and OH^- are small enough to penetrate (27, 28). The cation exchange capacity of kaolinite is much lower than that of 2:1 layer silicates such as montmorillonite [0.02 vs 1 equiv/kg (29)]; its origin and even its existence are still controversial (30, 31). Here, we assume, as is often the case, that isomorphic substitution in kaolinite results in a fixed surface charge on the basal (both siloxane and gibbsite) planes. Acid-base reactions take place both on the edges ($\equiv\text{AlOH}$ groups) and on the gibbsite basal planes (Al-O-Al groups) (32).

Clearly, kaolinite does not correspond exactly to the model solid we have examined. The permanent and variable charge distributions are not uniform on the surface of the clay; moreover, two different surfaces, the basal planes and the edges, are involved in the acid-base chemistry of the clay—in clear contradiction with our representation of the interface as an infinite plane. However, the essential feature of the

solid of model 1, i.e., the presence of both a permanent and a variable surface charge, is found in kaolinite, which may thus in a first approximation be adequately represented by model 1.

To test the applicability of the model, we examined a series of potentiometric curves of H-kaolinite at three different ionic strengths (Figure 5) published by Schindler et al. (33). The titration data exhibit unusual characteristics as compared to the “classic” curves usually obtained on oxides (contrast Figure 1 with Figure 5). Two (related) features are striking: (i) at acidic pH values, the clay is more protonated at lower ionic strength; at basic pH values, the situation is reversed (i.e., the lower the ionic strength, the less the deprotonation); (ii) the ZPC shows a slight but clear increase at lower I . The three titration curves of the clay thus never intersect; the extent of protonation of the solid being always greater at lower I (see Figure 5). This is in direct contrast with potentiometric data for oxides (see Figure 1).

Model 1 was applied to the potentiometric data of Schindler et al. (33) by adjusting the surface density of $\equiv\text{SOH}$ and $\equiv\text{X}^-$ groups and the $\text{p}K_{\text{a}}$ values of the acid-base groups to fit the titration data. The other parameters were fixed a priori or on the basis of other data (see Tables 1 and 2). The total surface density of $\equiv\text{SOH}$ was adjusted to fit the extent of protonation/deprotonation at low and high pH. The $\text{p}K_{\text{a}}$ values of the acid-base sites were then adjusted by trial and error to obtain the most satisfactory (to the eye) fit of the titration data. The permanent charge density was chosen to yield the correct increase in the surface density of protons as I decreases. The concentration of permanent charge obtained ($= 0.02$ equiv/kg) is in the range of what is usually found for kaolinite [i.e., 0.0–0.05 equiv/kg (30)]. (While adjusting more parameters would presumably yield a better fit of the data, it would defeat our purpose, which is to show that the structure of the model endows it with the appropriate qualitative behavior, not to optimize data fitting.) The specific surface area of the clay was taken to be $200\text{ m}^2/\text{g}$, about 20 times higher than the surface of $10.2\text{ m}^2/\text{g}$ measured by BET. This particular point is discussed later.

Despite its great simplicity, the model provides a satisfactory fit of the acid-base titration data of kaolinite at all ionic strengths (see Figure 5). In particular, the extent of protonation of the solid is correctly predicted to be always greater at $I = 0.01\text{ M}$ than at higher ionic strengths. This is because the surface charge is always negative, even at low pH, and the Coulombic attraction of H^+ is larger at low ionic strength over the whole pH range. This effect is quantified in Figure 4, which shows the potential variations with pH and ionic strength corresponding to the model parameters used for Figure 5.

Both the direction and the magnitude of the change in ZPC with decreasing I are satisfactorily reproduced. Again, the shift in ZPC is the direct consequence of a more negative potential at low I for the same surface density of X^- groups (see Figure 4).

Furthermore, the negligible effect on the acid-base titration curves of decreasing the ionic strength from $I = 1$ to $I = 0.1\text{ M}$ and the strong effect of changing it from 0.1 to 0.01 M , which are seen in the experimental data, are correctly predicted by the model. For $I = 0.1\text{ M}$, the surface potential is small over the entire pH range and can have only little effect on the acid-base properties of the solid (see Figure 4). Further increasing the ionic strength to $I = 1\text{ M}$ only further decreases the absolute value of the potential, and the titration curves at $I = 0.1$ and 1 M show little difference. On the contrary, decreasing the ionic strength to $I = 0.01\text{ M}$ induces a large increase in both the mean absolute value of the potential and the amplitude of its variations. The potential is then large enough to influence the acid-base

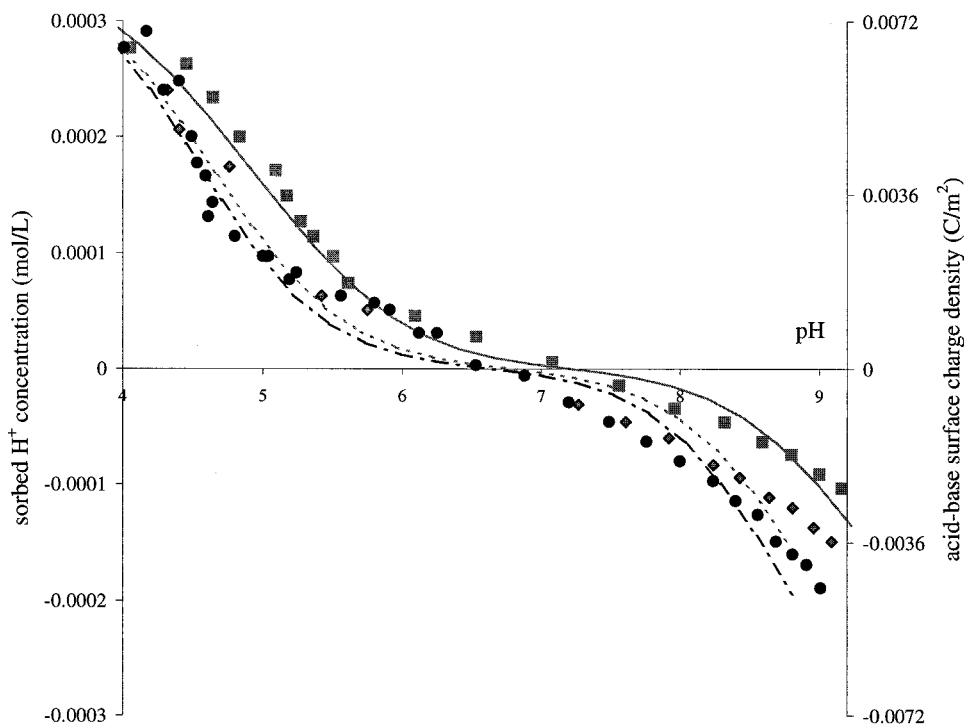


FIGURE 5. Acid–base titrations of kaolinite at three different ionic strengths: squares and —: $I = 0.01$ M; diamonds and - - -: $I = 0.1$ M; circles and - · - ·: $I = 1$ M. The fitting parameters for model 1 calculations (lines) are the same as for Figures 3 and 4. The data (symbols) are taken from Schindler et al. (33).

characteristics of the kaolinite, and the titration curve at $I = 0.01$ M is clearly different from the titration curves at higher I .

The effects of ionic strength described above depend greatly on the relative magnitude of the permanent and variable surface charge densities. For example, the acid–base titration curves should cross each other as I is varied if the absolute value of σ_{fix} is lower than $\sigma_{\text{var}}^{\text{max}}$ and the surface charge becomes positive at low pH. One should thus expect to observe different behaviors among different samples of kaolinite with varying extent of isomorphous substitution.

To obtain a satisfactory fit of the data, we had to increase the specific surface area of kaolinite by a factor of about 20 as compared to the surface measured by BET (33). If the BET value for the surface is used in the model, the effect of varying ionic strength on the acid–base curves is still qualitatively correct (i.e., at any pH, the surface is always more protonated at low I), but it is larger than what is actually seen in the data. Xie and Walther (28) have argued that the surface measured by BET is an underestimation of the real surface of kaolinite, the gas molecules being too big to access small channels along the edges where acid–base reactions may take place. According to these authors, the “real” surface would be 10–20 times higher than the BET surface. We think, however, that the apparent discrepancy between model and data may come chiefly from the oversimplification of the geometry of the kaolinite particle by the model. As pointed out earlier, two different surfaces, the surface basal gibbsite planes and the edges, are involved in the acid–base chemistry of the clay. The permanent negative charge—resulting from isomorphous substitution—is likely to be distributed chiefly along the basal planes. Furthermore, there is some evidence that most of that charge is on the surface siloxane planes, which may not have any acid–base properties (30, 31, 34). Clearly, spatial separation between permanent and variable charge is likely to weaken the effect of the negative potential resulting from the permanent charges on the acid–base groups. This may explain why our model can reproduce the data only in the case where the influence of the negative

charges is reduced by artificially increasing the surface area of kaolinite. A more elaborate electrostatic model with space separation of the charges, similar to that developed by Chang and Sposito for 2:1 clays (35, 36), may thus be needed to provide a physically and chemically satisfying representation of kaolinite.

Model 2. For our examination of model 2, we consider (anticipating on our application to montmorillonite) a high internal concentration of permanent charge: 1.02 equiv/L. We also choose a high concentration of acid–base groups per area of solid surface: $8.2 \times 10^{-2} \text{ C m}^{-2}$. The parameters chosen for model 2 are shown in Tables 1 and 2. (Because the model calculations are relatively insensitive to the parameters ϵ_s and V_L/V_P , which are poorly known, we have imposed $\epsilon_s(V_L/V_P) = \epsilon_w$, see eq 15.)

As seen in Figure 6, the log C –pH diagrams corresponding to model 2, with and without permanent internal charge, are qualitatively similar to those obtained for model 1 (see Figure 3). With no internal charge the ZPC is independent of I , and the apparent pK_a values become increasingly separated as I decreases. The introduction of a (high) permanent internal charge results in a much higher ZPC, and this effect is attenuated at high ionic strength. The ZPC is thus again pH-dependent (see Table 3).

The concentrations of H^+ that are sorbed inside the clay as a result of ion exchange become significant in model 2 at low pH and low ionic strength. In fact, as seen in Figure 6c, at $\text{pH} < 4$ and $I = 0.005$ M, the “exchanged” concentration of H^+ inside the solid calculated for our model dominates all the acid–base surface species.

The variations in surface potential with pH and I , which are responsible for the various shapes of the log C –pH diagrams of Figure 6, are shown in Figure 7. In the absence of an internal charge, the surface potential varies rapidly with pH at low ionic strength and much less at high ionic strength. In this case, the DDL model is very similar to the DL model, the two diffuse layers on both sides of the solid/water interface being symmetrical (see Figure 2).

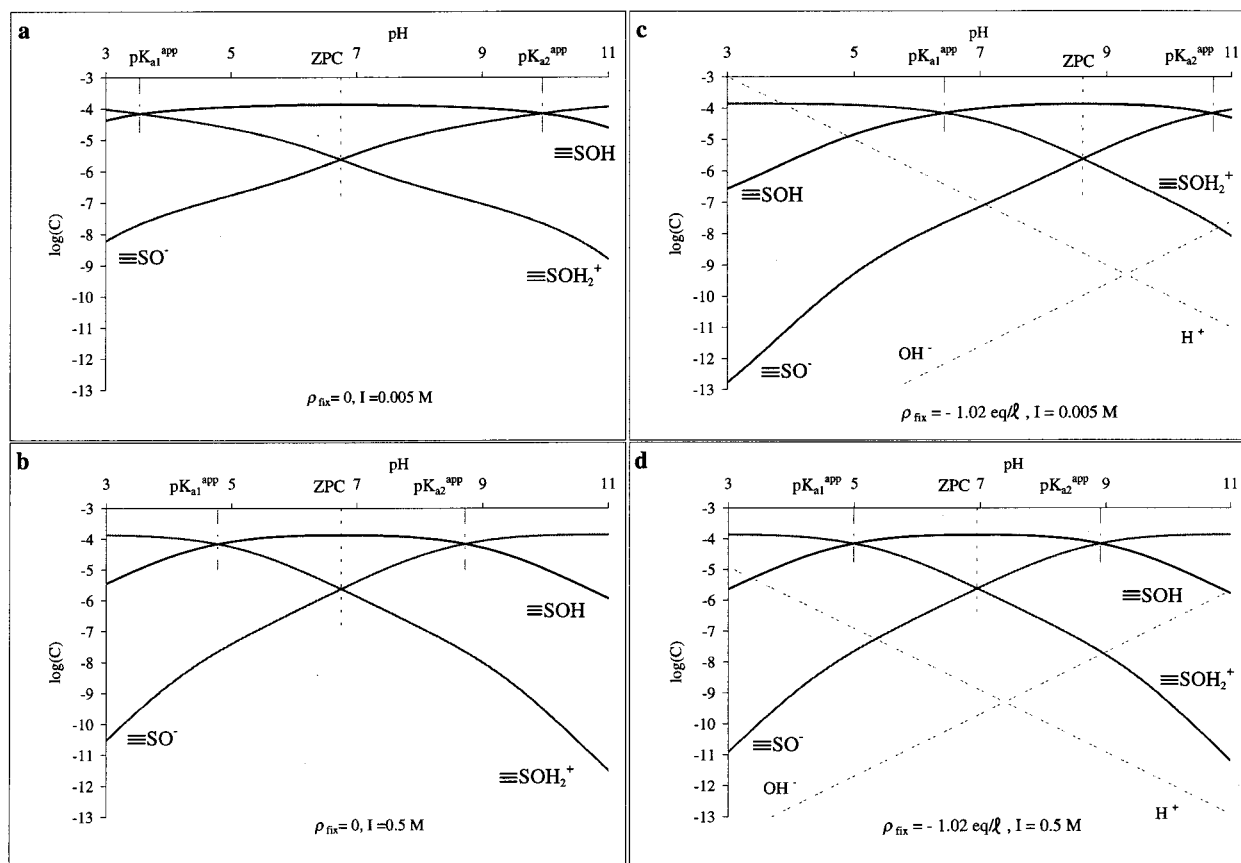


FIGURE 6. Log C –pH diagrams for acid–base surface species of a porous solid, with and without a permanent internal negative charge, at two different ionic strengths ($I = 0.005$ and 0.5 M). The model parameters are given in Tables 1 and 2. The dashed lines in panels c and d represent the concentrations of H^+ and OH^- sorbed in the solid by ion exchange. The concentration scale is in moles per liter of solution.

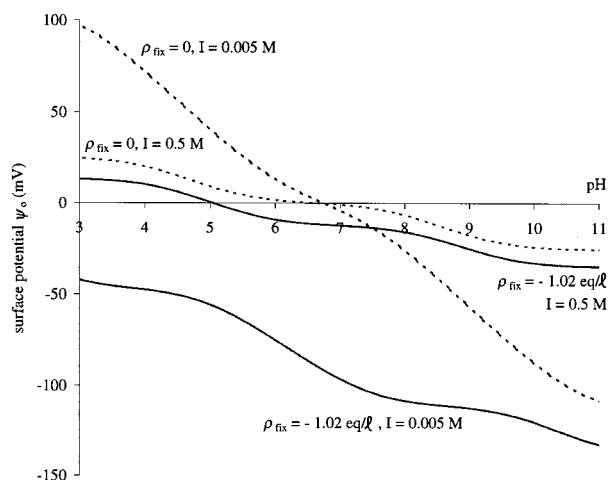


FIGURE 7. Surface potential versus pH at two ionic strengths ($I = 0.005$ and 0.5 M) for a porous solid, with a variable surface charge, and with or without a permanent negative internal charge. The model parameters are the same as for Figure 6. The dashed lines correspond to $\rho_{fix} = 0$; the continuous lines correspond to $\rho_{fix} = -1.02$ equiv/L.

In the presence of a large negative internal charge, the ψ vs pH graphs resemble those obtained in model 1 (compare Figures 4 and 7). The mean potential created in the bulk solid by the X^- groups is more negative at low I , and this is reflected in the surface potential. As a result, the surface potential is increasingly negative as the ionic strength is decreased. As seen in Figure 7, the variations of the surface potential with pH have a small amplitude, not only at high

ionic strength but also at low ionic strength. This is because the effective ionic strength at the interface is always high, being maintained between those in the bulk solid and solution.

Application to Montmorillonite. Montmorillonite is a 2:1 expandable clay; the layers, made of a succession of siloxane, gibbsite, and siloxane sheets, are separated by interlayers which are penetrable by water and electrolyte ions. The cation exchange capacity of montmorillonite resulting from isomorphous substitution is usually quite high, on the order of 1 equiv/kg (29). The gibbsite sheets of montmorillonite are sandwiched between siloxane sheets and are not available for acid–base reactions in the interlayers or the surface basal planes. The acid–base reactions of montmorillonite are thus presumed to occur predominantly at the exposed edges of the gibbsite layers.

A montmorillonite particle containing regularly spaced layers and interlayers does not correspond exactly to the model porous solid we have examined, because the porosity and charge are not homogeneously distributed. Montmorillonite, however, is penetrable by electrolyte ions and bears a permanent internal charge. A thermodynamic equilibrium should thus be established between ions in solution and ions in the interlayers of the clay, and this equilibrium should be governed by the internal potential of the clay. Indeed, Donnan models have been applied with success to describe cation exchange in clays (37). We thus hypothesize that montmorillonite may be represented as homogeneous porous solid with a uniform internal charge and potential and that model 2 may provide a satisfactory first-order description of its acid–base properties.

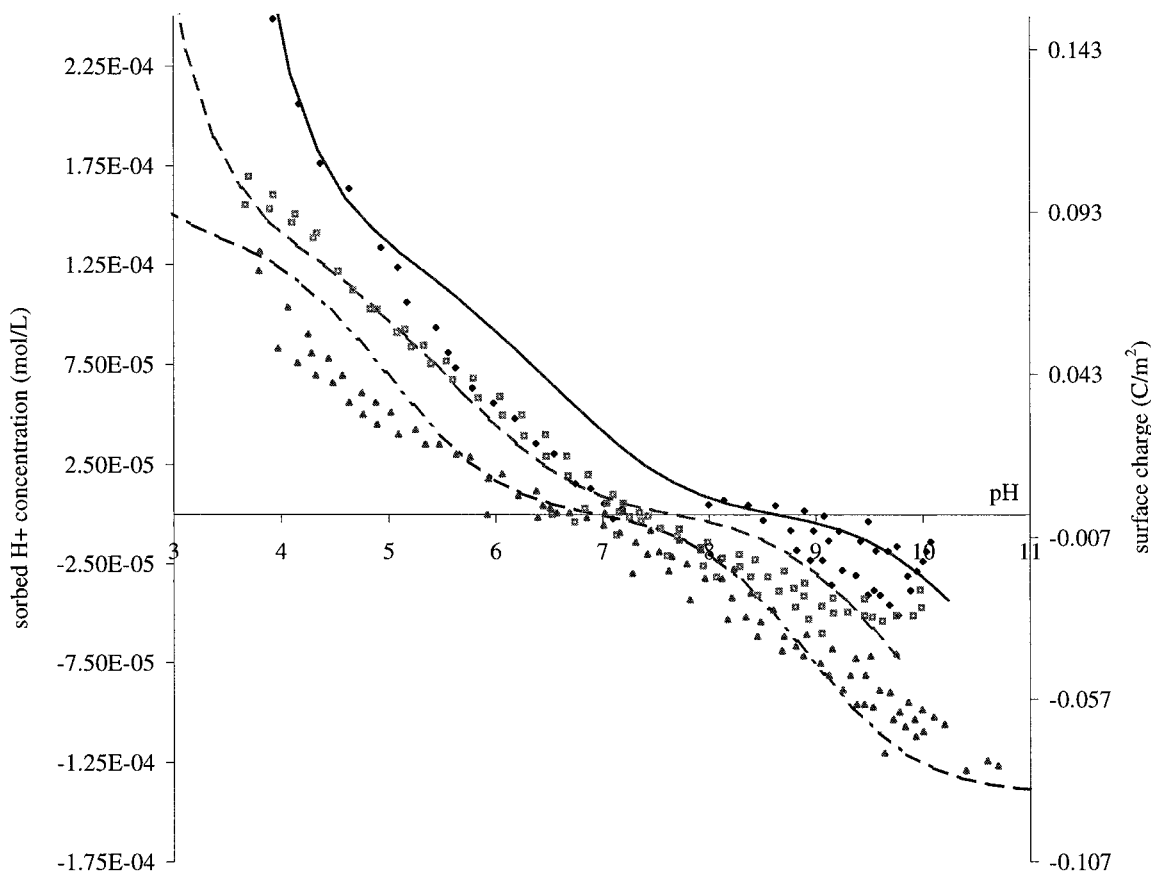


FIGURE 8. Acid–base titrations of montmorillonite at three different ionic strengths: diamonds and —: $I = 0.005$ M; squares and — —: $I = 0.05$ M; triangles and - · - ·: $I = 0.5$ M. The fitting parameters for model 2 calculations (lines) are the same as for Figures 6 and 7. The data (symbols) are from Wanner et al. (38). [Note: The scale on the right-hand side ($C\ m^{-2}$) is not applicable when, according to the model, the protonation of the solid is dominated by ion exchange inside the clay: $I = 0.005$ M, $pH < 4$.]

We applied model 2 to the acid–base titration data of Wanner et al. (38) obtained with Na-montmorillonite (see Figure 8). [Qualitatively similar data obtained by Baeyens and Bradbury (39) over a narrower range of ionic strengths have previously been modeled by us successfully (17).] The permanent charge density is calculated a priori from the cation exchange capacity of the clay (see Table 2). The concentration of acid–base sites on the surface and their intrinsic pK_a values are then adjusted to fit the data visually. The corresponding parameters are those that have been used in the illustration of model 2 in Figures 6–8. We ignore the possible swelling of the montmorillonite and maintain the physical parameters constant for all ionic strengths.

In view of the few adjustable parameters used, the model fits are quite satisfactory. As seen in Figure 8, the model successfully fits three important features of the experimental data:

- (i) An increase of the ZPC of nearly 2 pH units as the ionic strength is lowered from 0.5 to 0.005 M. This is a reflection of the large negative potential at low I (see Figures 6 and 7).
- (ii) A systematic upward displacement of the titration curve as I decreases. In particular at low pH, a lower ionic strength results in a higher surface charge, contrary to what is observed on oxides. According to our model, this is the result of the increasingly negative surface potential at low I . The influence of the larger negative internal potential resulting from a lower ionic strength (reflected in the lower ψ_o vs pH curve in Figure 7) dominates over the diminished ability of the surface to build up a positive charge (reflected in the larger amplitude of ψ_o variation in Figure 7).
- (iii) The titration curves at various ionic strengths are nearly parallel to each other, unlike titration curves on oxides

that flatten as the ionic strength decreases. This is a reflection of the relatively parallel and attenuated variations of ψ_o versus pH at various I shown in Figure 7.

Particularly remarkable in Figure 8 is the large increase in excess protons in the solid observed at $I = 0.005$ M and $pH < 4$. In the model, this increase corresponds to the dominance of the H^+ sorbed into the solid by ion exchange, as shown in Figure 6. It is no surprise that H^+ , like Na^+ , should be subjected to ion exchange in montmorillonite and that this effect should become important when H^+ becomes a significant fraction of the ionic content of the medium. Clearly such an effect must be included in any model of the acid–base chemistry of 2:1 layer clays.

As shown here, the net effects of a pH-independent charge on the acid–base chemistry of solids can be rather pronounced. In particular, it can lead at low pH to an increasing sorption of protons with decreasing ionic strength, an effect opposite to that observed on oxides. It also leads to an upward displacement of the ZPC with decreasing I and to titration curves that are nearly parallel to each other rather than intersect at a common ZPC. Similar effects are observed on clays such as kaolinite and montmorillonite. Simple models taking into account the presence of a pH-independent charge may thus provide an adequate description of the acid–base properties of clays in the same way and with the same limitations that the usual surface complexation model can describe the acid–base properties of oxides.

Acknowledgments

The authors thank James J. Morgan for his friendly and critically important comments. Financial support from EPA, NSF, ONR, and IFREMER is gratefully acknowledged.

Literature Cited

- (1) Gouy, G. *J. Phys. Radium* **1910**, *9*, 457–468.
- (2) Chapman, D. L. *Philos. Mag.* **1913**, *25*, 475–481.
- (3) Stern, O. *Z. Elektrochem.* **1924**, *30*, 508–516.
- (4) Dzombak, D. A.; Morel, F. M. M. *Surface Complexation Modeling*; Wiley-Interscience: New York, 1990.
- (5) Huang, C. P.; Stumm, W. *J. Colloid Interface Sci.* **1973**, *43*, 409–420.
- (6) Ronngren, L.; Sjöberg, S.; Sun, Z.; Forsling, W.; Schindler, P. W. *J. Colloid Interface Sci.* **1991**, *145*, 396–404.
- (7) Van Cappellen, P.; Charlet, L.; Stumm, W.; Wersin, P. *Geochim. Cosmochim. Acta* **1993**, *57*, 3505–3518.
- (8) Carroll-Webb, S. A.; Walther, J. V. *Geochim. Cosmochim. Acta* **1988**, *52*, 2609–2623.
- (9) Turner, G. D.; Zachara, J. M.; McKinley, J. P.; Smith, S. C. *Geochim. Cosmochim. Acta* **1996**, *60*, 3399–3414.
- (10) Lyklema, J. *J. Electroanal. Chem.* **1968**, *18*, 341–348.
- (11) Perram, J. W.; Hunter, R. J.; Wright, H. J. L. *Chem. Phys. Lett.* **1973**, *23*, 265–269.
- (12) Perram, J. W.; Hunter, R. J.; Wright, H. J. L. *Aust. J. Chem.* **1974**, *27*, 461–475.
- (13) Verwey, E. J. W.; Niessen, K. F. *Philos. Mag.* **1939**, *28*, 435–446.
- (14) Grimley, T. B. *Proc. R. Soc. London A* **1950**, *201*, 40–61.
- (15) Grimley, T. B.; Mott, N. F. *Discuss. Faraday Soc.* **1947**, *1*, 3–11.
- (16) Bartschat, B.; Cabaniss, S. E.; Morel, F. M. M. *Environ. Sci. Technol.* **1992**, *26*, 284–294.
- (17) Kraepiel, A. M. L.; Keller, K.; Morel, F. M. M. *J. Colloid Interface Sci.* Submitted for publication.
- (18) Donnan, F. G. *Z. Elektrochem.* **1911**, *17*, 572–581.
- (19) Dzombak, D. A.; Hudson, R. J. M. In *Aquatic Chemistry: Interfacial and Interspecies Processes*; Huang, C. P., O'Melia, C. R., Morgan, J. J., Eds.; American Chemical Society: Washington, DC, 1995; pp 59–94.
- (20) Westall, J. C.; Zachary, J. L.; Morel, F. M. M. *Mineql. A computer program for the calculation of chemical equilibrium composition of aqueous systems*; Massachusetts Institute of Technology: Cambridge, 1976.
- (21) Westall, J. In *Particulates in Water*; Kavanaugh, M. C., Leckie, J. O., Eds.; American Chemical Society: Washington, DC, 1980; pp 33–44.
- (22) Keller, K.; Kraepiel, A. M. L.; Morel, F. M. M. *Clayeq1—A Subroutine for the Simulation of Sorption Processes on Clays*; Department of Civil Engineering and Operation Research, Princeton University: Princeton, NJ, In preparation.
- (23) Stumm, W.; Morgan, J. J. *Aquatic Chemistry*; Wiley-Interscience: New York, 1996.
- (24) Hohl, H.; Sigg, L.; Stumm, W. In *Particulates in Water*; Kavanaugh, M. C., Leckie, J. O., Eds.; American Chemical Society: Washington, DC, 1980; pp 1–31.
- (25) Tunney, J.; Detellier, C. *Clays Clay Miner.* **1994**, *42*, 473–476.
- (26) van Olphen, H. *An introduction to Clay Colloid Chemistry*; Wiley-Interscience: New York, 1977.
- (27) Huertas, F. J.; Chou, L.; Wollast, R. *Geochim. Cosmochim. Acta* **1998**, *62*, 417–431.
- (28) Xie, Z.; Walther, J. V. *Geochim. Cosmochim. Acta* **1992**, *56*, 3357–3363.
- (29) Sposito, G. *The Chemistry of Soils*; Oxford University Press: Oxford, 1989.
- (30) Schroth, B.; Sposito, G. *Clays Clay Miner.* **1997**, *45*, 85–91.
- (31) Kim, Y.; Cygan, R. T.; Kirkpatrick, R. J. *Geochim. Cosmochim. Acta* **1996**, *60*, 1041–1052.
- (32) Zhou, Z.; Gunter, W. D. *Clays Clay Miner.* **1992**, *40*, 365–368.
- (33) Schindler, P. W.; Liechti, P.; Westall, J. C. *Neth. J. Agric. Sci.* **1987**, *35*, 219–230.
- (34) Ferris, A. P.; Jepson, W. B. *J. Colloid Interface Sci.* **1975**, *51*, 245–259.
- (35) Chang, F.-R. C.; Sposito, G. *J. Colloid Interface Sci.* **1994**, *163*, 19–27.
- (36) Chang, F.-R. C.; Sposito, G. *J. Colloid Interface Sci.* **1996**, *178*, 555–564.
- (37) Arnold, P. W. In *The Chemistry of Soil Constituents*; Greenland, D. J., Hayes, M. H. B., Eds.; Wiley-Interscience: New York, 1978; pp 355–404.
- (38) Wanner, H.; Albinsson, Y.; Karnland, O.; Wieland, E.; Wersin, P.; Charlet, L. *Radiochim. Acta* **1994**, *66/67*, 157–162.
- (39) Baeyens, B.; Bradbury, M. H. *J. Contam. Hydrol.* **1997**, *27*, 199–222.
- (40) McBride, M. B. *Environmental Chemistry of Soils*; Oxford University Press: Oxford, 1994.
- (41) Hsi, C. D.; Langmuir, D. *Geochim. Cosmochim. Acta* **1985**, *49*, 1931–1941.

Received for review March 24, 1998. Revised manuscript received June 1, 1998. Accepted June 15, 1998.

ES9802899